

Modeling 3D Hydrogen Diffusion And Localized Hydride Formation In Zirconium Alloy Cladding Using High Fidelity Multi-Physics Coupled Codes.

Ahmed Aly¹, Kyle Gamble², Maria Avramova¹, Richard Williamson², Kostadin Ivanov¹

1-North Carolina State University: 2500 Stinson drive, Raleigh, NC, 27695, USA. amaly@ncsu.edu, mnavramo@ncsu.edu, knivanov@ncsu.edu.

2- Idaho National Laboratory: Fuels Modeling and Simulation Dept. Idaho Falls, ID, 83415, USA. kyle.gamble@inl.gov, richard.williamson@inl.gov.

Abstract - The high-speed water coolant in LWRs constitutes a corrosive environment that interacts with the fuel cladding. These interactions result in the release of hydrogen which might be absorbed in the cladding. Once picked-up in the cladding, the hydrogen forms a solid solution with the zircaloy alloy cladding and diffuse inside it. The hydrogen diffusion process is driven by two forces; The concentration and the temperature gradients determined by Fick's law and the Soret effect respectively. Once the concentration of hydrogen has reached the terminal solid solubility of precipitation, it starts to precipitate as hydrides. Hydrides can embrittle the cladding and result in cracks that propagate to the limit at which the integrity of the cladding is compromised. Therefore, it is important to model the diffusion of hydrogen and the local formation of hydrides to be able to quantify their effects on the cladding. A model of this process is implemented in the BISON fuel performance code.

The modeling process in this work was performed using three multi-physics codes; MPACT, COBRA-TF and BISON to model neutronics, thermal hydraulics, and fuel performance respectively. The codes were coupled using the coupling driver TIAMAT. The results of the performed computations were fed to a stand-alone BISON 3D model in which the diffusion and precipitation of hydrogen were observed for a modeled two months of irradiation. The hydrogen tended to diffuse to the lower temperature regions and precipitate. The diffusion and precipitation processes were much enhanced at locations in the cladding around a fuel inter-pellets gap.

I. INTRODUCTION

Nuclear reactors are complex systems used for generating energy from nuclear fission. The fission process results in the production of fission fragments that might be radioactive or represent a risk to the public health. Therefore, these fragments should be retained within the fuel. The fuel cladding serves as the first barrier against the release of such fission products to the environment outside the nuclear power plant. The fuel cladding should preserve its integrity during the whole lifetime of the fuel inside the reactor and during its storage as a spent fuel.^[1]

Zirconium alloys are extensively used as a cladding for Light Water Reactors (LWRs). Zirconium based alloys are preferred because of their low thermal neutron absorption cross sections, relatively high melting temperature, and good corrosion and fracture resistance. Zircaloy-2 (Zr-1.5Sn-0.12Fe-0.1Cr-0.05Ni in wt.%) is used as a cladding material for Boiling Water Reactors (BWRs) while Zircaloy-4 (Zr-1.5Sn-0.2Fe-0.1Cr-0.007Ni in wt.%) is used as a cladding for Pressurized Water Reactors (PWRs).^[2]

One of the factors that might affect the integrity of the fuel cladding is the formation of hydride precipitates.^[3] The high velocity water used as a coolant for LWRs is a highly corrosive environment to the zirconium cladding. This corrosive action involves the oxidation of the cladding accompanied by the release of hydrogen.^[4] A fraction of this

released hydrogen can be picked-up by the cladding to form a solid solution. The hydrogen tends to diffuse from higher concentrations to lower concentrations regions (Fick's law) and from higher temperatures to lower temperatures regions (Soret effect).^[5] Depending on the concentration and temperature, the hydrogen may form localized hydride precipitates that might embrittle the cladding locally. This makes the cladding vulnerable to cracking and its integrity might be compromised.^[3] At a specific axial height and azimuthal angle the local hydride concentration might be very high, forming a weak point in the cladding. Therefore, a three-dimensional (3D model) is needed to be able to quantify this local effect. A 2D (R-Z) model might average out this local effect and underestimate its impact on the cladding.

The purpose of this work is to provide a computational model and corresponding data that will be used in validating the prediction of 3D hydrogen distribution in the cladding once there are accurate experimental data to compare with. A model of hydrogen behavior and distribution inside the cladding has been implemented in the BISON fuel performance code.^[6] This code is used for the prediction and the follow-up validation of the 3D distribution of the hydrogen in the cladding.

To be able to model the hydrogen distribution in 3D, a case in which the outer cladding temperature is azimuthally asymmetric was considered. This was done by performing multi-physics coupled calculations using the neutronics

code MPACT^[7], thermal hydraulics code CTF^[8] along with a 2D BISON model. These three codes are coupled using the TIAMAT^[9] coupling driver being developed within the Virtual Environment for Reactor Applications (VERA)^[10] within the Consortium for Advanced Simulation of Light Water Reactors (CASL).^[11] Several fuel rods with different enrichments in the vicinity of a guide tube were modeled. The difference of enrichments and the guide tube resulted in an azimuthally varying cladding temperature. The data generated from the coupled codes were used as boundary conditions for a stand-alone, single-rod, BISON model to generate 3D data for the distribution of hydrogen in the studied fuel rod.

II. HYDROGEN MODEL DESCRIPTION

1. Oxidation Mechanisms Of Zircaloy

The corrosion of Zircaloy alloys due to interactions with the water coolant leads to the formation of an oxide layer on the outer surface of the fuel cladding.^[12] This process results in a weight gain of the cladding due to the formation of a thick oxide layer which falls in two periods. Initially, the corrosion of Zircaloy begins with the formation of a thin black oxide film. This happens in the initial pre-transitional period in which the rate of weight gain of the cladding follows a semi-cubical function with a decreasing rate in weight gain. After this initial period, A transition state to a gray or white oxide occurs. the thickness of the cladding increases and the weight gain increases linearly.

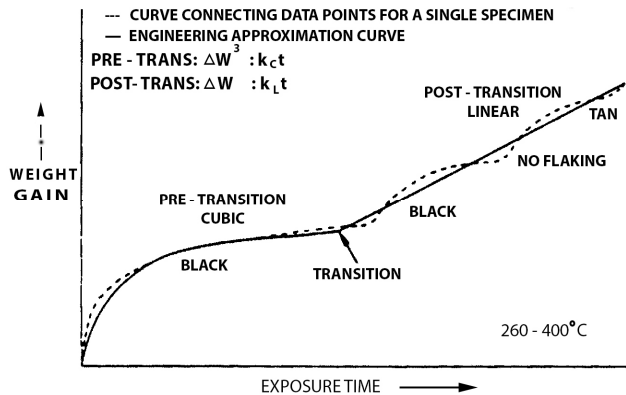
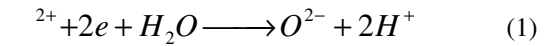


Fig. 1. Schematic representation of corrosion of zircaloy-2 and zircaloy-4 in the temperature range of 260 to 400 °C.^[13]

As the oxide thickens, the mean size of the crystallite increases. When the oxide thickness reaches a value of approximately 2 μm, the second period begins.^[14] In this period, the oxidation rate increases rapidly in a linear fashion. This increase is due to the formation of pores and cracks in the oxide layers that makes it easier for more oxygen to diffuse from the coolant to the interface layer between the metal and the oxide of zirconium. The

evolution of the oxide size as a function of weight gain of the cladding with exposure time is illustrated in Fig. 1.

The formed oxide layer will have different structures depending on the oxygen concentration and the temperature of the medium around the cladding. Below 871 °C, two structures exist. A layer of alpha-Zr containing oxygen in solid solution is formed and followed by an outer layer of zirconia. Above 982 °C, many layers can exist but three are most identified. An inner layer of metal containing some transformed beta zirconium is formed and followed by an intermediate layer of alpha layer that is oxygen stabilized. An external layer of zirconia is formed in contact with the coolant.^[12] The mechanisms by which oxidation occurs can be separated into two reactions occurring simultaneously.^[15] The first one is:



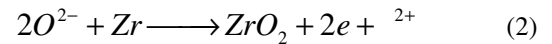
where:

\square^{2+} is an anionic vacancy in the oxide lattice,

2e are two free electrons formed at the oxide metal interface,

O^{2-} is the oxygen ion formed at the water-oxide interface.

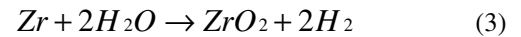
In this interaction, anionic vacancy and two electrons interact with water to form an oxygen ion and two hydrogen ions. Then the oxygen ion will diffuse through the oxide film until it reaches the metallic zircaloy alloy where it will interact with zirconium to form an extra zirconium dioxide molecule with the release of two electrons and an anionic vacancy in the following reaction:



The vacancies and the electrons diffuse to the outer surface of the cladding through the oxide film to reach the waterside and the cycle of oxidation and corrosion of the cladding continues. The hydrogen ions produced in this reaction can be picked-up in the cladding or flow with the water until it recombines with an oxygen ion.

2. Hydrogen Pickup

The two reactions in equations (1) and (2) can be combined in the following form to represent the waterside corrosion reaction of the zirconium alloy cladding and the corresponding hydrogen release:



A fraction of the released hydrogen will be absorbed through the oxide layer to form a solid solution inside the cladding.^[16] The average total concentration of hydrogen C_H

in the cladding is proportional to the thickness of the oxide layer and is written on the following form:

$$C_H = \frac{4f}{R_{PB}} \frac{\delta}{L - \delta} \frac{M_H}{M_{Zr}} \quad (4)$$

where:

f is the hydrogen pickup fraction,
 R_{PB} is the Pilling-Bedworth ratio for ZrO_2 (=1.56),
 δ is the oxide layer thickness
 L is the initial thickness of the cladding,
 M_H and M_{Zr} are the molecular weights of hydrogen and zirconium respectively.^[17]

This fraction of hydrogen that is instantaneously absorbed in the cladding was found to be a strong function of alloying elements and the exposure time.^[18] The study of the pickup fraction is not the main goal of this work. In BISON, the user specifies a fixed instantaneous hydrogen pickup fraction, so that the average total concentration of hydrogen C_H (including dissolved hydrogen and hydrogen as ZrH_x) in the cladding is roughly proportional to the thickness of the oxide layer. On average, around 15% of the released hydrogen from this reaction might be absorbed in the cladding forming a solid solution in the zirconium alloy.^[5] This ratio is what was used in the studied hydrogen model.

3. Hydrogen Diffusion In The Cladding

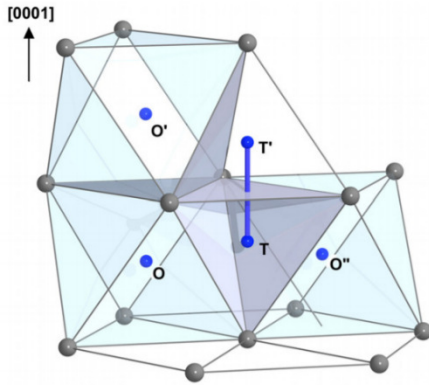


Fig. 2. Structure of hcp Zr with octahedral (O, O', O'') and tetrahedral (T and T') interstitial sites.^[19]

Once the hydrogen is picked-up in the metallic cladding, it dissolves in α -Zr interstitial lattice sites. Tetrahedral locations and octahedral locations are the favorite interstitial locations to which hydrogen tends to diffuse.^[19] Those locations can be seen in Fig. 2. Experimental studies of the site preference of hydrogen in Zr have been performed by Khoda-Bakhsh and Ross.^[20] They employed neutron diffraction to study site occupancy

in Zr for a hydrogen concentration of 3.2 at%. In the literature, it is often stated that hydrogen occupies tetrahedral sites in Zr. This is plausible since ϵ - ZrH_2 , which is the end-point of hydrogenating zirconium, has a distorted calcium fluoride structure where all tetrahedral sites of the face-centered cubic (fcc) host lattice are occupied by H atoms. The hydrogen can then diffuse in the solid solution of the zirconium matrix. This diffusion process is governed by two forces: the concentration gradient (Fick's law) and the temperature gradient (Soret's effect).

The hydrogen diffuses in the cladding from areas of high concentration to areas of low concentration according to Fick's law:

$$J_{Fick} = -D \nabla N \quad (5)$$

where:

J_{Fick} = diffusion flux of hydrogen in zirconium due to concentration gradients as described by Fick's Law,
 N = concentration of hydrogen in the solid solution,
 D = diffusion coefficient of hydrogen in zirconium. This coefficient is temperature dependent and is governed by Arrhenius law:

$$D(T) = -D_0 \cdot \exp\left(\frac{-Q_D}{RT}\right) \quad (6)$$

The coefficients in equations (6) were determined by Kearns for hydrogen^[21] to be:

$$D_0 = 7.9 \cdot 10^{-7} \frac{m^2}{s} \quad (7)$$

and Q_D , the activation energy which was found to be:

$$Q_D = 4.49 \cdot 10^4 \frac{J}{mol} \quad (8)$$

The hydrogen also diffuses from areas of high temperatures to areas of low temperatures (Soret effect):

$$J_{Soret} = -\frac{DNQ}{RT^2} \nabla T \quad (9)$$

where:

J_{Soret} = diffusion flux of the hydrogen due to temperature and concentration gradients,
 R = gas constant,
 T = temperature in degree kelvin,
 Q = heat of transport for hydrogen in zirconium,
 D = diffusion coefficient of hydrogen in zirconium.

The overall flux of hydrogen due to the temperature and concentration gradients can be evaluated by combining equations (5) and (9) to obtain:

$$J_D = -D\nabla N - \frac{DNQ}{RT^2} \nabla T \quad (10)$$

4. Hydride Precipitation And Dissolution

With hydrogen diffusing in the cladding, it might at certain locations exceed its terminal solid solubility of precipitation (TSSP).^[22] In that case, some of the hydrogen might precipitate as zirconium hydrides. The TSSP is a function of the temperature and is given by the following equation:

$$TSSP = 138746e^{\frac{-4145.7}{T}} \quad (11)$$

The precipitated hydrides can dissolve back to the solution if the concentration of hydrogen in the solid solution drops to a lower limit known as the terminal solid solubility of dissolution (TSSD):

$$TSSD = 106446.7e^{\frac{-4328.67}{T}} \quad (12)$$

where: temperature is in Kelvin.

Fig. 3 illustrates both quantities as a function of temperature.

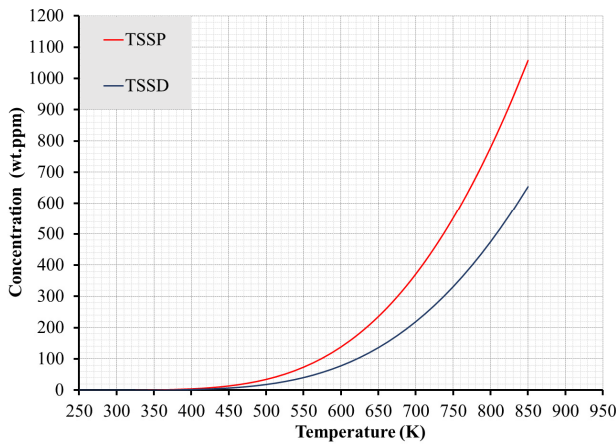


Fig. 3. TSSP and TSSD concentrations as a function of temperature.

It is shown in Fig. 3 that for the same temperature value, there are two different values for TSSP and TSSD. This creates some form of hysteresis effect when the hydrogen precipitates or dissolves. The reason for that effect is that

the precipitation occurs by a nucleation and growth process. It is necessary to create an initial nucleus for the precipitate to grow hence, the higher TSSP value.

III. MULTI-PHYSICS COUPLED CALCULATIONS

The modeling of the hydrogen behavior in this study involved several multi-physics codes that were coupled together. Using them provided the advantage of the high fidelity in the model's results. The performed computations involved three codes. MPACT is a neutron transport code used within VERA. The code provides modeling capabilities for 3-D method of characteristics (MOC), 2-D/1-D time-dependent transport, and traditional 2-D lattice physics capabilities. The COBRA-TF (COolant Boiling in Rod Array – Two Fluid) code also known as CTF is a multi-dimensional sub-channel thermal hydraulics code. It is being utilized in the CASL project for high-fidelity thermal-hydraulics calculations. BISON is the Idaho National Laboratory's multi-dimensional (2D and 3D), finite-element-based, fuel performance code. BISON can model temperature distributions, fission product swelling, densification, thermal and irradiation creep, mechanical properties, and fission gas production. Those codes were coupled by TIAMAT, a multi-physics coupling code that was developed within CASL project as part of the VERA. It was used to couple the three single physics codes described above to perform high fidelity coupled calculations.

MPACT is used to calculate the power inside the fuel rods and pass it to BISON for fuel performance calculations. BISON will return the fuel rod temperature to MPACT that will use it to update the cross sections inside the fuel. CTF will pass the coolant temperature and density to MPACT that will be used to update the cross sections inside the coolant. The code will pass the cladding outer surface temperature to BISON that will be used as a boundary condition for the fuel rods. And, in return, CTF will take the heat flux from BISON to calculate the flow conditions and heat transfer to update the coolant temperature. The coupling scheme used in TIAMAT is shown in Fig. 4.

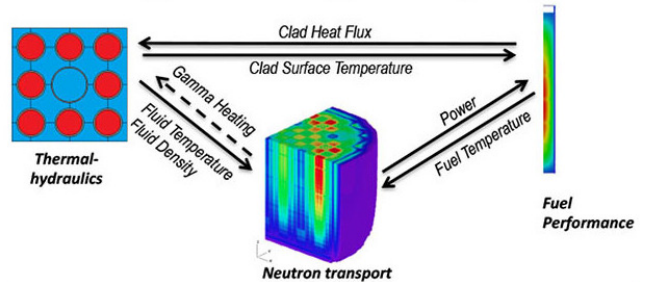


Fig. 4. TIAMAT multi-physics coupling scheme.^[23]

IV. THE VERA MODEL

To investigate the azimuthal distribution of hydrogen, the outer cladding temperature should be azimuthally dependent. VERA is used to generate such a case in which a 3x3 sub-assembly is modeled. The sub-assembly contains eight fuel pins of different enrichments and a guide tube. The flow area is divided to 16 subchannels plotted in Fig. 5.

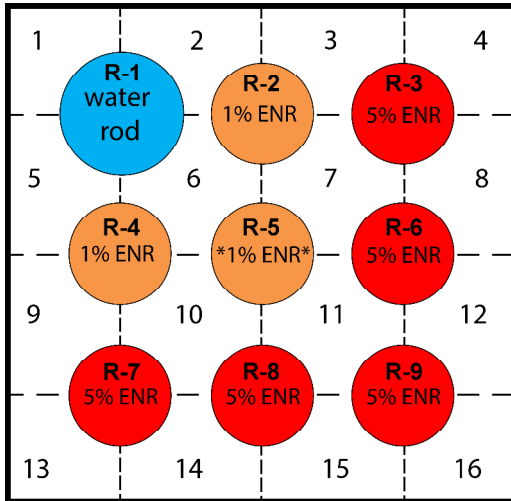


Fig. 5. The VERA modeled 3x3 subassembly (horizontal view).

The input parameters of VERA are scaled to the chosen subassembly. Such parameters are the array power, mass flow rate, spacer grids weight, etc. A summary of some of the important parameters used within the VERA model are summarized in Table I.

Table I. Subassembly VERA input parameters.

Parameter	Value
System parameters:	
Reactor Type	PWR
Subassembly power (MW)	0.535
Average linear heat rate (kW/m)	18.5
Coolant pressure (MPa)	15.5
Mass flow rate (kg/s)	3.2
Inlet temperature (K)	566
Fuel pin parameters:	
Fuel type	UO ₂
Fuel density (g/cm ³)	10.257
Cladding type	Zircaloy-4
Cladding density (g/cm ³)	6.56
Fill gas	Helium
Initial fill gas pressure (MPa)	2.6
Geometry:	
Fuel pellet radius (m)	0.004096
Cladding outer radius (m)	0.00475
Cladding thickness (m)	0.00057

Pin pitch (m)	0.0126
Active fuel height (m)	3.6
Core height (m)	4.06

The coupled computations were performed according to the scheme in Fig. 4. The rod of interest in Fig. 5 is R-5 in the center marked with two asterisks and has a 1% enrichment. It is surrounded by a group of rods having 5% and 1% enrichments and a guide tube. R-5 is divided to four quadrants. Each quadrant is part of one of the subchannels 6,7,10 and 11. The different rod types in those subchannels resulted in a different average coolant temperature in each of them. This leads to four different average outer cladding surface temperature for the same rod R-5 in each of the four quarters.

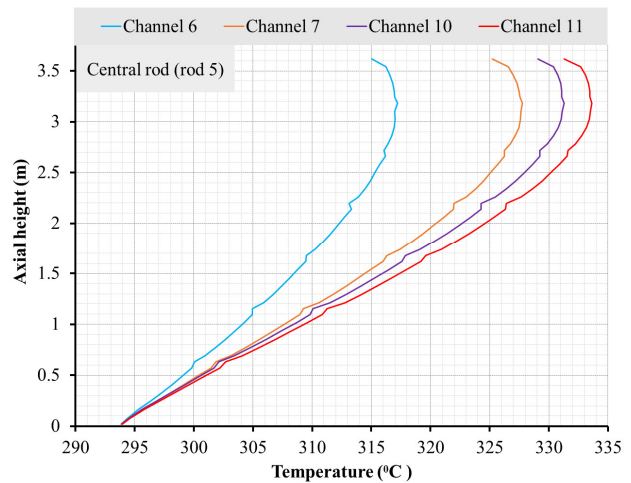


Fig. 6 Axial average outer cladding temperature profile in the four coolant subchannels surrounding the R-5 rod.

This situation is depicted in Fig. 6 along the axial length of the fuel rod. It is noticed as well that the variation of the temperature between the different subchannels increases with the axial elevation. Having a larger gradient will increase the potential for the diffusion of hydrogen due to the Soret effect. It is also noticed that the axial temperature profile increase does not vary smoothly at every point on the axial height. There are several locations where there is a sudden perturbation in the cladding temperature. This happens at locations where a spacer grid is located. As the axial location becomes farther away from the spacer grid, the temperature follows the expected axial profile.

V. STAND-ALONE 3D BISON MODEL

It would be computationally impractical approach to try to model a full-length fuel rod in 3D using BISON. Therefore, a section of interest in the fuel rod around a spacer grid was extracted and modeled. The chosen spacer grid was the highest one covering the active length of the

fuel at a height of 322 cm. The reason for this choice is to have a temperature gradient that is high enough to allow the investigation of the hydrogen diffusion and precipitation. Eleven discrete fuel pellets were modeled with the cladding outer surface temperatures as boundary conditions extracted from CTF. Table II summarizes the axial locations at which the temperature boundary conditions were computed by CTF and the corresponding temperature values.

Table II. CTF cladding temperature boundary conditions in Kelvin in each subchannel surrounding the modeled rod section.

Axial height (m)	Ch 6	Ch.7	Ch.10	Ch.11
3.183	590.23	600.76	604.3	606.65
3.242	589.96	600.55	604.07	606.47
3.301	589.93	600.49	604.1	606.48

The average discrete temperatures provided by CTF had to be converted to a continuous domain on the cladding surface in order to be able to use them in the stand-alone 3D BISON model. To be able to do this, a parsed function was created and used to linearly interpolate the temperatures at the outer surface of the fuel between the specific CTF average temperatures as shown in Fig. 7.

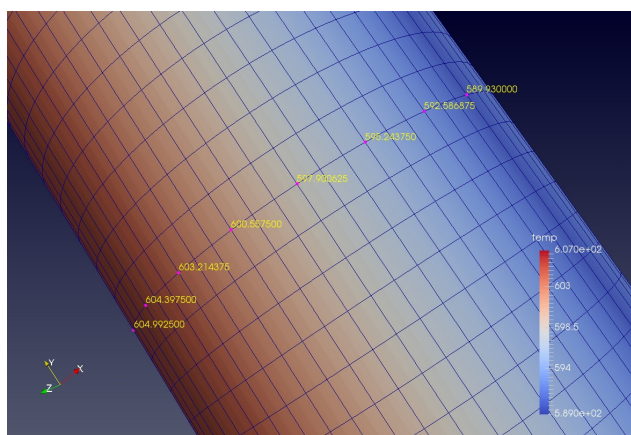


Fig. 7. Azimuthally asymmetric outer cladding temperature profile.

The mesh on the extracted section of the fuel pin was created with CUBIT/TRELIS. A coarse mesh was used in the beginning to test the 3D model and modifications to it. The mesh was later refined to provide a higher resolution and more accurate representation of the hydride formation in the cladding.

In order to investigate the formation of hydrides, the concentration of hydrogen has to increase beyond the TSSP limit at least at the lowest temperatures in the model domain. These temperatures are on the outer surface of the

cladding. In this case study, the outer cladding surface temperature ranged from about 590 K to 606.7 K. Using equation (11), we got a corresponding TSSP values of 123 to 149.5 wt.ppm respectively. Starting the simulations with zero wt.ppm concentration of hydrogen would not lead to the formation of hydrides in the cladding. The hydrogen pickup process would have taken a long time to allow this to happen. It is costly from a computation resources point of view to model this situation. An alternative approach was to assume a specific initial concentration of hydrogen in the cladding. This concentration should be high enough to allow the hydrogen precipitation process to take place. In this case, the initial hydrogen concentration was taken to be 150 ppm by weight.

VI. RESULTS

The simulation time was taken to be 5×10^6 seconds, which is around two months of irradiation, at a linear heat rate of 18.5 kW/m. In Fig. 8 the hydrogen distribution is depicted at the end of the simulation. Hydrogen in the solid solution migrated to the lower temperature regions of the cladding where the concentration reached 132.5 wt.ppm. This value is lower than the initial concentration of 150 wt.ppm due to the formation of hydrides. The effect of the azimuthal variation of the temperature is more clear when comparing Fig. 7 and Fig. 8. It can be seen the lower the temperature the higher the hydrogen concentration and vice versa.

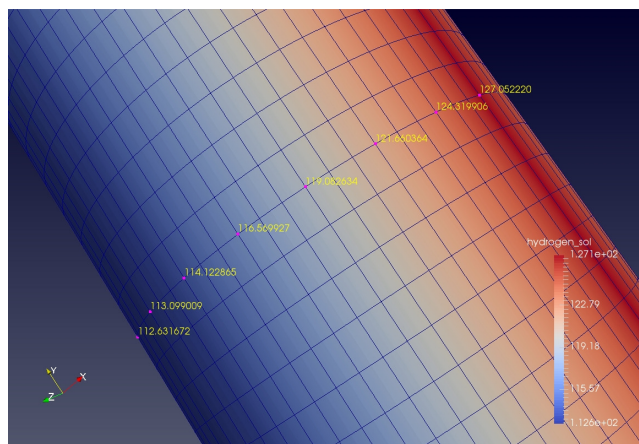


Fig. 8. 3D hydrogen distribution in the cladding.

Axially, as shown in Table II, The change of the temperature due to the space grid is lower than 1 K. This does not considerably affect the axial hydrogen distribution within the modeled section of the fuel pin. The regions in the cladding in contact with the inter-pellets gap in the fuel will be of relatively lower temperatures as shown in Fig. 9. Those regions are favorable for the hydrogen to diffuse to then precipitate as hydride. Several rings of higher concentrations of hydrides are noticed on the outer surface

of the cladding around those locations as shown in Fig. 10. The concentration of hydrogen in the hydrides follows the same pattern of its concentration in the solid solution. In fact, the formation of hydrides is a consequence to the diffusion of hydrogen in the solid solution. That is because hydrogen concentration must first increase at certain locations above the TSSP value before it is possible for hydrides to be formed.

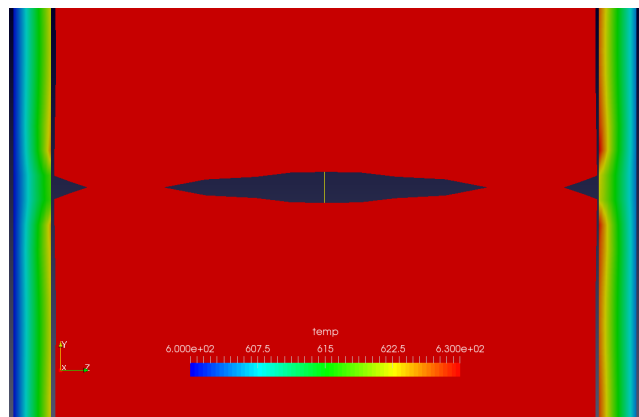


Fig. 9 Temperature profile in the cladding around inter-pellets gap in the fuel rod.

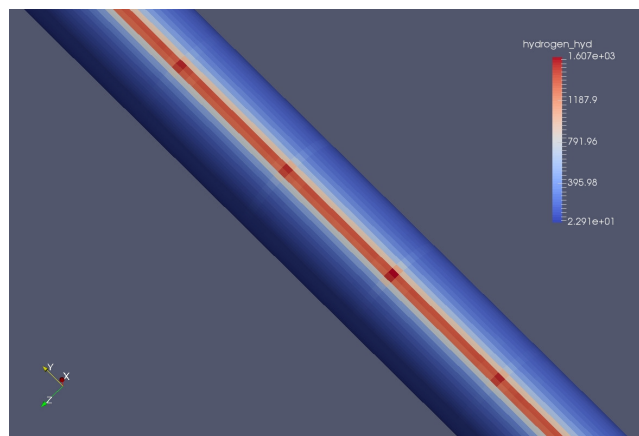


Fig. 10. 3D hydrides distribution in the cladding.

Fig. 11 shows the hydrogen distribution in hydrides along an axial line on the outer surface of the cladding. The spikes in hydrides concentration corresponds to locations around the inter-pellets gaps. The lower hydride concentrations are in regions where the cladding is in contact with the right cylindrical section of the fuel pellets.

The azimuthal and radial distribution of the hydrogen in the solid solution and in the hydrides was investigated in a radial slice of the cladding. This slice was taken at an inter-pellets location where the distribution of hydrides reached a local axial maximum. Fig. 12 depicts the temperature profile in this slice. The temperature is higher on the inner side of

the cladding and decreases radially to reach the boundary condition temperatures. It varies azimuthally as well because of the imposed boundary conditions. This temperature variation will affect the hydrogen and hydrides distributions as shown in Fig. 13 and Fig. 14.

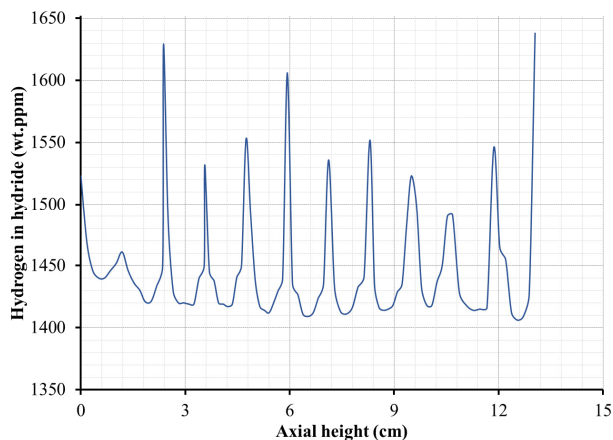


Fig. 11 Axial distribution of hydrogen in hydrides along the modeled section of the fuel pin.

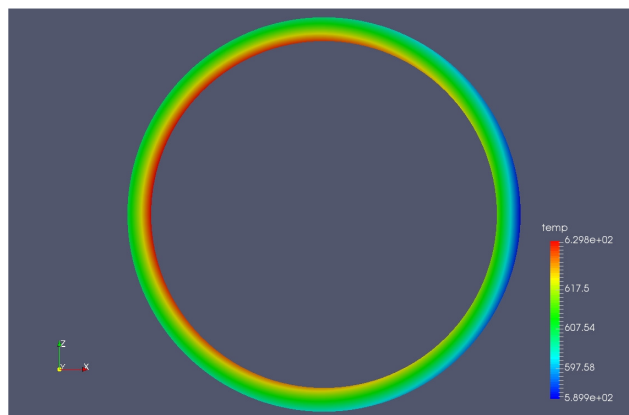


Fig. 12 Temperature profile in a horizontal slice in the modeled section of the fuel.

In Fig. 13 the hydrogen distribution in the slice is shown. Hydrogen migrates radially to the relatively cooler outer periphery of the cladding and azimuthally to the regions with lower temperature. As the hydrogen migrates to the lower temperature regions, the concentration in the warmer regions of the cladding falls below TSSD. Therefore, hydrogen cannot precipitate in those regions. Hydride precipitates was formed in regions with lower temperatures i.e. higher concentration of hydrogen and lower TSSP values as shown in Fig. 14.

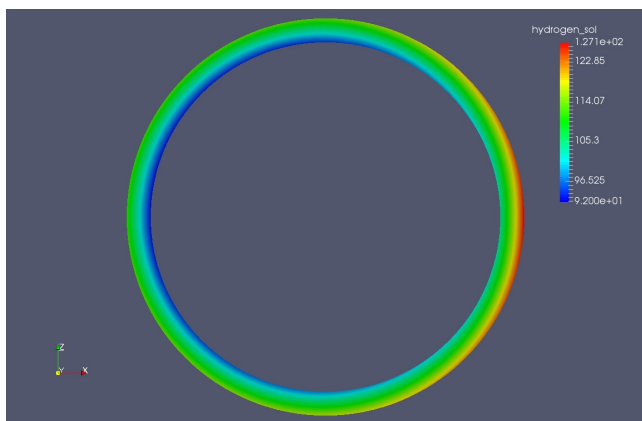


Fig. 13. Hydrogen distribution in solid solution at a slice of the cladding.

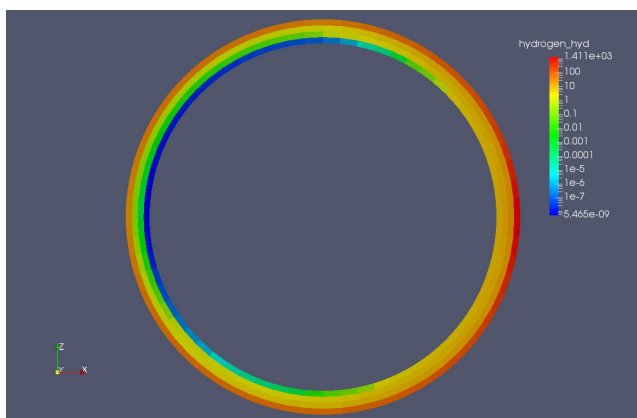


Fig. 14 Hydrogen distribution in hydrides at a slice of the cladding.

VII. CONCLUSIONS

Modeling the hydrogen diffusion is an important aspect of maintaining the cladding as an important barrier against the leakage of fission products and minor actinides to the environment. This is important during the lifetime of the fuel inside the reactor and during the wet and dry storage of the fuel elements. Corrosive reactions of the cladding with the water coolant results in the release of hydrogen in the coolant. A fraction of this hydrogen is picked-up by the cladding and diffuses inside it. This process is controlled by the temperature and concentration gradients inside the cladding.

If the hydrogen concentration exceeded a certain concentration limit (TSSP) at a certain temperature, it starts to precipitate on the form of stationary hydrides. Those hydrides can dissolve again to the solid solution if the concentration dipped below another lower concentration limit (TSSD). The formed hydride can embrittle the cladding and results in cracking nodes inside it that can propagate with the stresses. This effect is a local one and it

is of interest to model the diffusion of hydrogen and its precipitation locally rather than modeling the average behavior which might screen out higher local concentrations that will contribute to the cracking of the cladding.

A VERA model was created in which the temperature varies azimuthally in the cladding. Coupled calculations between BISON-CTF-MPACT were performed and driven by the coupling driver TIAMAT. The azimuthally asymmetric cladding temperatures were extracted from CTF output and fed to the stand-alone BISON 3D model as boundary conditions. Computations based on this model were performed to investigate the hydrogen behavior within the cladding. The hydrogen diffusion was dependent on the temperature and concentration gradients. Locations where temperatures were low and hydrogen concentration was high tended to have a higher concentration of hydrogen in the precipitated hydrides. This should help, once proper validation experiments are performed, to predict the effect of the hydrogen and the hydride precipitates on the integrity of the cladding during its different life stages from in-core to dry cask storage.

ACKNOWLEDGMENT

The work reported in this paper is supported by the US DOE NEUP Project 13-5180 entitled “Three-dimensional fuel pin model validation by prediction of hydrogen distribution in cladding and comparison with experiment.”

The authors would like to express their appreciation to Kevin Clarno and the TIAMAT team for their assistance.

REFERENCES

1. INSAG, “Defense in Depth in Nuclear Safety,” IAEA publications (1996).
2. A. SAWATZKY, C.E. ELLS, “Understanding Hydrogen in Zirconium” *Zirconium in the nuclear industry: Twelfth international symposium* ASTM STP 1354, West Conshohocken, Pennsylvania, pp 32-48, (2000).
3. K. S. CHAN, “An Assessment of Delayed Hydride Cracking in Zirconium Alloy Cladding Tubes under Stress Transients,” *Int. Mater. Rev.*, 58(6), pp 349-373, (2013).
4. C. E. COLEMAN, D. HARDIE, “The Hydrogen Embrittlement of Alpha-Zirconium Review,” *J. Less-common. Met.*, 11, pp. 168-185 (1966).
5. O. COURTY, “Hydrogen Distribution in Zircaloy under a Temperature Gradient: Modeling, Simulations, and Experiment,” M.Sc. in Nuclear Engineering, The Pennsylvania State University, (2013).
6. BISON Team, “BISON theory manual: The equations behind nuclear fuel analysis,” INL-2015, Idaho National Laboratory (2015).
7. MPACT Team, “MPACT Theory Manual, Version 2.0.0”, Tech. Rep. CASL-U-2015-0078-000, Oak Ridge National Laboratory and University of Michigan (2015).

8. R. SALKO, M. AVRAMOVA, "COBRA-TF Sub-Channel Thermal Hydraulics Code Theory Manual," CASL-2015, Consortium for Advanced Simulation of Light water reactors (2015).
9. K. T. CLARNO, et al., "High Fidelity Modeling of Pellet-Clad Interaction Using the CASL Virtual Environment for Reactor Applications," *Proc. The ANS Joint International Conference on Mathematics and Computation (M&C 2015), Supercomputing in Nuclear Applications (SNA) and the Monte Carlo (MC) Method.*, Nashville, Tennessee, (2015).
10. S. PALMTAG, "Demonstration of Neutronics Coupled to Thermal-Hydraulics for a Full-Core Problem Using VERA," CASL-U-2013-0196-000, Oak Ridge National Laboratory (2013).
11. S. PALMTAG, A. GODFREY, "VERA Common Input User Manual," CASL-2015, Consortium for Advanced Simulation of Light water reactors (2015).
12. IAEA, "Waterside Corrosion of Zirconium Alloys in Nuclear Power Plants", IAEA-TECDOC-996, (1998).
13. E. HILLNER "Corrosion of Zirconium Based Alloys: an Overview", *Zirconium in the nuclear Industry, Third conference* ASTM STP 633, pp 211-235, (1977).
14. A. ALMARSHAD, "A Model for Waterside Oxidation of Zircaloy Fuel Cladding in Pressurized Water Reactors", Ph.D. Thesis in nuclear engineering, Oregon State University, (1990).
15. B. PARFENOV, V. GERASIMOV, G. VENDIKTOVA, "Corrosion of Zirconium and Zirconium Alloys" IPST Press, (1969).
16. D. S. STAFFORD, "Multidimensional Simulations of Hydrides During Fuel Rod Life Cycle," *J. Nucl. Mater.* 466, pp 362-372, 2015.
17. O. COURTY, A. T. MOTTA, and J. D. HALES, "Modeling and Simulation of Hydrogen Behavior in Zircaloy-4 Fuel Cladding," *J. Nucl. Mater.* 452, pp 311-320 (2014).
18. A. COUET, A. T. MOTTA, and R. J. COMSTOCK, "Hydrogen Pickup Measurements in Zirconium Alloys: Relation to Oxidation Kinetics," *J. Nucl. Mater.*, 451, pp 1-13 (2014).
19. M. CHRISTENSEN, et al, "H in α -Zr and in Zirconium Hydrides: Solubility, Effect on Dimensional Changes, and the Role of Defects", *J. Phys: Condens. Matter* 27, (2015).
20. K. BAKHSH, D. Ross, "Determination of the Hydrogen Site Occupation in the α Phase of Zirconium Hydride and in the α and β Phases of Titanium Hydride by Inelastic Neutron Scattering", *J. Phys. F: Met. Phys*, 12, (1981).
21. J. KEARNS, "Diffusion Coefficient of Hydrogen in Alpha Zirconium, Zircaloy-2 and Zircaloy-4", *J. Nucl. Mater.* 53, pp 330-338, (1972).
22. M. MANKOSA, "Modeling of Hydrogen and Hydride Formation in Zirconium Alloy Cladding Using High-Fidelity Multi-Physics Coupled Codes," M.Sc. in Nuclear Engineering, The Pennsylvania State University, (2015).
23. <http://www.casl.gov/image-gallery.shtml>, Last checked February 13, 2017.